RESEARCH ARTICLE SUMMARY

CARBON CYCLE

Influence of El Niño on atmospheric CO_2 over the tropical Pacific Ocean: Findings from NASA's OCO-2 mission

A. Chatterjee,* M. M. Gierach, A. J. Sutton, R. A. Feely, D. Crisp, A. Eldering, M. R. Gunson, C. W. O'Dell, B. B. Stephens, D. S. Schimel

INTRODUCTION: The Orbiting Carbon Observatory-2 (OCO-2) is NASA's first satellite designed to measure atmospheric carbon dioxide (CO_2) with the precision, resolution, and coverage necessary to quantify regional carbon sources and sinks. OCO-2 launched on 2 July 2014, and during the first 2 years of its operation, a major El Niño occurred: the 2015–2016 El Niño, which was one of the strongest events ever recorded.

El Niño and its cold counterpart La Niña (collectively known as the El Niño–Southern Oscillation or ENSO) are the dominant modes of tropical climate variability. ENSO originates in the tropical Pacific Ocean but spurs a variety of anomalous weather patterns around the globe. Not surprisingly, it also leaves an imprint on the global carbon cycle. Understanding the magnitude and phasing of the ENSO-CO_2 relationship has important implications for improving the predictability of carbon-climate feedbacks.

The high-density observations from NASA's OCO-2 mission, coupled with surface ocean CO_2 measurements from NOAA buoys, have provided us with a unique data set to track the atmospheric CO_2 concentrations and unravel the timing of the response of the ocean and the terrestrial carbon cycle during the 2015–2016 El Niño.

RATIONALE: During strong El Niño events, there is an overall increase in global atmospheric CO_2 concentrations. This increase is predominantly due to the response of the terrestrial carbon cycle to El Niño–induced changes in weather patterns. But along with the terrestrial component, the tropical Pacific Ocean also plays an important role. Typically, the tropical Pacific Ocean is a source of CO_2 to the atmosphere due to equatorial upwelling that brings CO_2-rich water from the interior ocean to the surface. During El Niño, this equatorial upwelling is suppressed in the eastern and the central Pacific Ocean, reducing the supply of CO_2 to the surface. If CO_2 fluxes were to remain constant elsewhere, this reduction in ocean-to-atmosphere CO_2 fluxes should contribute to a slowdown in the growth of atmospheric CO_2. This hypothesis cannot be verified, however, without large-scale CO_2 observations over the tropical Pacific Ocean.

RESULTS: OCO-2 observations confirm that the tropical Pacific Ocean played an early and important role in the response of atmospheric CO_2 concentrations to the 2015–2016 El Niño. By analyzing trends in the time series of atmospheric CO_2, we see clear evidence of an initial decrease in atmospheric CO_2 concentrations over the tropical Pacific Ocean, specifically during the early stages of the El Niño event (March through July 2015). Atmospheric CO_2 concentration anomalies suggest a flux reduction of 26 to 54% that is validated by the NOAA Tropical Atmosphere Ocean (TAO) mooring CO_2 data. Both the OCO-2 and TAO data further show that the reduction in ocean-to-atmosphere fluxes is spatially variable and has strong gradients across the tropical Pacific Ocean.

ON OUR WEBSITE

Read the full article at http://dx.doi.org/10.1126/science.aam5776

During the later stages of the El Niño (August 2015 and later), the OCO-2 observations register a rise in atmospheric CO_2 concentrations. We attribute this increase to the response from the terrestrial component of the carbon cycle—a combination of reduction in biospheric uptake of CO_2 over pan-tropical regions and an enhancement in biomass burning emissions over Southeast Asia and Indonesia. The net impact of the 2015–2016 El Niño event on the global carbon cycle is an increase in atmospheric CO_2 concentrations, which would likely be larger if it were not for the reduction in outgassing from the ocean.

CONCLUSION: The strong El Niño event of 2015–2016 provided us with an opportunity to study how the global carbon cycle responds to a change in the physical climate system. Space-based observations of atmospheric CO_2, such as from OCO-2, allow us to observe and monitor the temporal sequence of El Niño–induced changes in CO_2 concentrations. Disentangling the timing of the ocean and terrestrial responses is the first step toward interpreting their relative contribution to the global atmospheric CO_2 growth rate, and thereby understanding the sensitivity of the carbon cycle to climate forcing on interannual to decadal time scales. ■

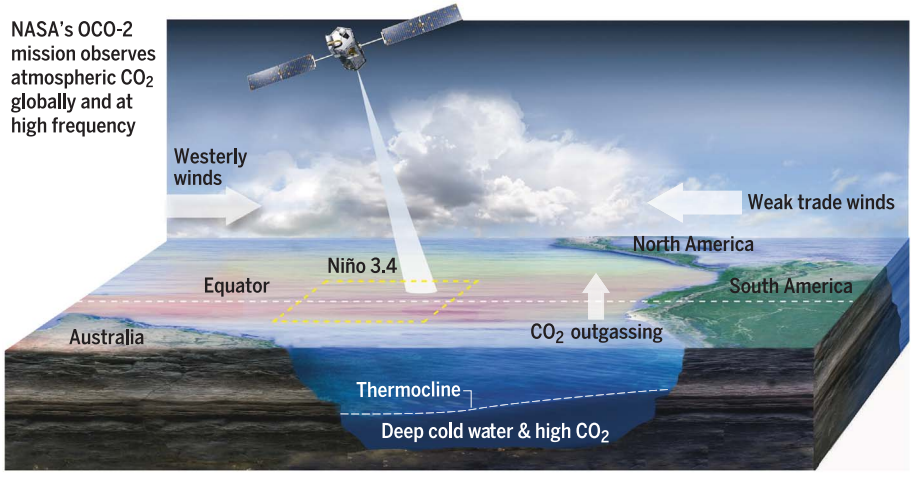

NASA's carbon sleuth tracks the influence of El Niño on atmospheric CO_2. The tropical Pacific Ocean, the center of action during an El Niño event, is shown in cross section. Warm ocean surface temperatures are shown in red, cooler waters in blue. The Niño 3.4 region, which scientists use to study the El Niño, is denoted by yellow dashed lines. As a result of OCO-2's global coverage and 16-day repeat cycle, it flies over the entire region every few days, keeping tabs on the changes in atmospheric CO_2 concentration.

The list of author affiliations is available in the full article online.
*Corresponding author. Email: abhishek.chatterjee@nasa.gov
Cite this article as A. Chatterjee *et al.*, *Science* **358**, eaam5776 (2017). DOI: 10.1126/science.aam5776

RESEARCH ARTICLE

CARBON CYCLE

Influence of El Niño on atmospheric CO_2 over the tropical Pacific Ocean: Findings from NASA's OCO-2 mission

A. Chatterjee,[1,2]* M. M. Gierach,[3] A. J. Sutton,[4,5] R. A. Feely,[4] D. Crisp,[3] A. Eldering,[3] M. R. Gunson,[3] C. W. O'Dell,[6] B. B. Stephens,[7] D. S. Schimel[3]

Spaceborne observations of carbon dioxide (CO_2) from the Orbiting Carbon Observatory-2 are used to characterize the response of tropical atmospheric CO_2 concentrations to the strong El Niño event of 2015–2016. Although correlations between the growth rate of atmospheric CO_2 concentrations and the El Niño–Southern Oscillation are well known, the magnitude of the correlation and the timing of the responses of oceanic and terrestrial carbon cycle remain poorly constrained in space and time. We used space-based CO_2 observations to confirm that the tropical Pacific Ocean does play an early and important role in modulating the changes in atmospheric CO_2 concentrations during El Niño events—a phenomenon inferred but not previously observed because of insufficient high-density, broad-scale CO_2 observations over the tropics.

The El Niño–Southern Oscillation (ENSO) is the dominant mode of tropical climate variability on interannual to decadal time scales (*1*–*5*) and is correlated with large interannual variability in global atmospheric CO_2 concentrations (*6*–*19*). Studying the response of the carbon cycle to this natural climate phenomenon is critical to understanding and quantifying the sensitivity of the carbon cycle to climate variability and, by extension, to climate in general (*20*). Although the ENSO cycle originates in the equatorial Pacific, its impact on the carbon cycle is felt globally as a result of its regional teleconnections (*21*, *22*) and influences on atmospheric and ocean circulation, precipitation, temperature, and fire emissions (*1*, *23*–*25*). Partitioning the response of the constituent components of the carbon cycle to a complete El Niño event has been challenging because of the limited number of CO_2 observations over tropical land and ocean regions.

Observations of atmospheric CO_2 from space provide a global view of the carbon cycle that can be used to describe phenomena that have been previously pieced together from sparse in situ data. NASA's Orbiting Carbon Observatory-2 (OCO-2) mission was successfully launched on 2 July 2014 and started providing science data in early September 2014 (*26*). Within the first 2 years of operation of the OCO-2 mission, a major El Niño (the warm phase of the ENSO) occurred (*27*–*30*). We provide an approach for studying the temporal sequence of El Niño–induced changes in global CO_2 concentrations, using observations from the OCO-2 mission that are validated with CO_2 data from the Tropical Atmosphere Ocean (TAO) moored array. We see a response from the tropical Pacific Ocean during the early stages of an El Niño event and a lagged (and much larger) terrestrial signal as the El Niño reaches maturity.

[1]Universities Space Research Association, Columbia, MD, USA. [2]NASA Global Modeling and Assimilation Office, Greenbelt, MD, USA. [3]Jet Propulsion Laboratory, California Institute of Technology, Pasadena, CA, USA. [4]NOAA Pacific Marine Environmental Laboratory, Seattle, WA, USA. [5]Joint Institute for the Study of the Atmosphere and Ocean, University of Washington, Seattle, WA, USA. [6]Colorado State University, Fort Collins, CO, USA. [7]National Center for Atmospheric Research, Boulder, CO, USA.
*Corresponding author. Email: abhishek.chatterjee@nasa.gov

El Niño and the global carbon cycle

Correlations between the atmospheric CO_2 growth rate and El Niño activity have been reported since the 1970s (*6*–*8*, *31*, *32*), although the magnitude and timing of the responses of the ocean and terrestrial components remain poorly constrained (*33*). Here, the word terrestrial includes changes in biospheric productivity (respiration and photosynthesis) as well as biomass burning (fires). Following previous strong El Niño events (for example, the 1982–1983 and 1997–1998 El Niño events), methods for measuring the atmospheric CO_2 response to the ENSO were based on in situ atmospheric CO_2 observations at a handful of surface stations that transect the tropical Pacific, including Mauna Loa, Christmas Island, and American Samoa (*8*, *34*), as well as shipboard transect measurements (*12*, *35*, *36*). The annual growth rate of atmospheric CO_2 measured at these remote stations and other sites around the globe has shown remarkable correlation with ENSO indices, with a rapid increase in atmospheric CO_2 associated with the late stage of an El Niño event (*19*, *37*). Measurements of the ocean response to El Niño events have been based on studies looking at in situ observations—for example, surface ocean pCO_2 observations from ships of opportunity (*12*), moorings (*38*, *39*), or targeted field campaigns during El Niño events (*9*, *10*, *40*, *41*)—and a variety of mechanistic ocean models (*23*, *42*–*46*).

The overall increase in the release of CO_2 to the atmosphere during strong El Niño events has been attributed to a decrease in biospheric uptake of CO_2 (e.g., due to drying of tropical land regions and an increase in plant and soil respiration) combined with enhanced fire emissions. In recent years, this has led to a growing body of literature (*47*–*54*) concluding that ENSO-mediated variability in tropical net land primary productivity is what primarily influences the atmospheric CO_2 growth rate. A handful of studies (*24*, *55*, *56*) have disputed any consistent or coherent response from the land component during El Niño events, thus highlighting the high level of uncertainty and disagreement within the carbon cycle community.

The El Niño CO_2 signature should have a tropical Pacific Ocean component as well, with opposite sign to the terrestrial response (*10*, *13*, *33*). During strong El Niño events, there is a large-scale weakening of the easterly trade winds and suppression of eastern equatorial Pacific upwelling (indicated by a deeper thermocline) that reduces the supply of cold, carbon-rich waters to the surface (Fig. 1). This reduces the usual strong outgassing of CO_2 from this region (*42*–*46*, *57*–*68*)—typically on the order of ~0.4 to 0.6 Pg C $year^{-1}$ to the atmosphere—by ~40 to 60% during an El Niño event (*9*–*12*, *33*, *36*, *63*, *68*). If net fluxes were to remain constant elsewhere, these substantial net air-sea CO_2 anomalies should lead to a reduction in the growth rate of atmospheric CO_2, at least during the early stages of El Niño.

Understanding these variations in atmospheric CO_2, their timing, and the underlying processes that cause them has been of great interest within the carbon cycle community (*1*, *10*–*13*, *15*, *20*, *33*, *55*). Integrating information from ocean- and atmosphere-based estimates and modeling studies, we now know that the combined and opposing effects of ocean and terrestrial responses contribute to El Niño–related variations in atmospheric CO_2 (*33*). However, there is limited understanding about the role of the ocean response. This is of crucial importance because typically the interannual variability (IAV) in the growth rate of atmospheric CO_2 is used to constrain the climate sensitivity of land carbon fluxes (Υ_{LT}) (*20*, *69*); however, if a component of the IAV is being modified by ocean fluxes, then these inferences of Υ_{LT} need to be reconsidered.

Because of the few surface CO_2 monitoring stations over the center of action (i.e., tropical Pacific Ocean), it has been challenging to directly observe the timing and changes in flux of CO_2 from the ocean to the atmosphere that affect the atmospheric CO_2 growth rate during an El Niño event. Efforts to analyze the data from distant measurement locations tend to identify the enhanced CO_2 fluxes from the terrestrial carbon cycle, which

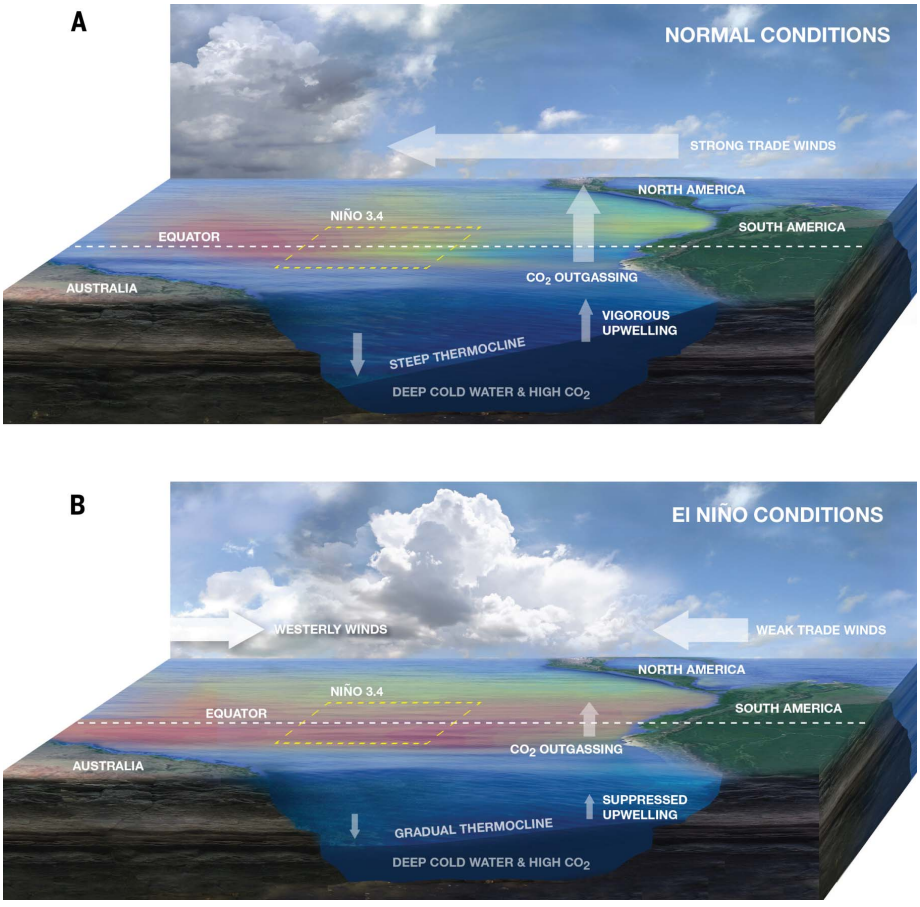

Fig. 1. Schematic of the mechanistic differences between normal and El Niño conditions and associated carbon response over the tropical Pacific Ocean. (**A**) normal conditions; (**B**) El Niño conditions. Warm ocean surface temperatures are denoted in red, cooler waters in blue. During El Niño conditions, easterly trade winds weaken and westerly wind bursts occur. In association with the shift in wind regimes, the western tropical Pacific warm pool moves eastward and the slope of the thermocline flattens in the central and eastern tropical Pacific. This suppresses upwelling of cold, carbon-rich waters in the central and eastern tropical Pacific, reducing the magnitude of CO_2 outgassing into the atmosphere. Also shown are changes in atmospheric convection, wherein convection shifts eastward in response to eastward displacement of western tropical Pacific warm pool waters.

dominate during the later stages of El Niño. The high-density, broad-scale observations of CO_2 from OCO-2 provide a valuable tool to partition the ocean and terrestrial carbon cycle responses to El Niño.

Time series of X_{CO_2} anomalies during the 2015–2016 El Niño

OCO-2 observations describe the column-averaged CO_2 dry-air mole fraction (X_{CO_2}). More details regarding the OCO-2 mission, data features, and X_{CO_2} retrievals are provided in (*26*, *70*, *71*); see (*72*) for validation of X_{CO_2} via comparisons to a ground-based network.

El Niño events are identified by warm sea surface temperature (SST) anomalies in precise regions of the tropical Pacific Ocean, with the most commonly used being the Niño 3.4 region (5°S to 5°N, 170° to 120°W). Shown in Fig. 2, A and B, is the trend in X_{CO_2} anomaly (*71*) for the Niño 3.4 region and its temporal evolution relative to two ENSO indices (*73*), including the Oceanic Niño Index (ONI, derived from SST anomalies in the Niño 3.4 region) and the Southern Oscillation Index (SOI, derived from observed sea-level pressure differences between Tahiti and Darwin, Australia). The 2015–2016 El Niño began around March 2015 and reached its peak over the central Pacific between November 2015 and January 2016 (*30*). The X_{CO_2} anomaly (Fig. 2B) shows two distinct periods over the entire El Niño event: (i) the onset phase of El Niño (spring and summer 2015), and (ii) the mature or peak phase of El Niño (fall 2015 onward). We attribute the negative X_{CO_2} anomaly during the first phase to a reduction in local CO_2 outgassing from the tropical Pacific Ocean; we argue that the positive trend in X_{CO_2} anomaly during the second phase reflects an increase in atmospheric CO_2 concentrations due to terrestrial sources (i.e., a combination of reduced vegetation uptake across pan-tropical regions and enhanced biomass burning emissions from Southeast Asia and Indonesia). The time series in Fig. 2B shows the space-based CO_2 data set documenting the response of the carbon cycle (both oceanic and terrestrial) during an entire El Niño event, capturing both the onset and the mature phase and the transition between them. The timing of the OCO-2 launch was extremely fortuitous in this regard.

Deriving the X_{CO_2} anomalies required observations taken by both NASA's OCO-2 and the Japan Aerospace Exploration Agency's (JAXA) Greenhouse Gases Observing Satellite (GOSAT) (*74*) mission. The short OCO-2 record makes it impossible to fit a long time series and calculate anomalies; hence, we used data from the GOSAT mission (operating since January 2009) to generate the X_{CO_2} climatology. The OCO-2 team retrieved X_{CO_2} data from the first 7 years of GOSAT observations, using the same retrieval algorithm that generated the OCO-2 data product (*71*). Continuous global coverage from these two missions allowed us to stitch together a long time series of X_{CO_2} over remote regions, such as the tropical Pacific Ocean (figs. S1 and S2). However, the use of two data sources (i.e., GOSAT and OCO-2) can incur errors in the analyses due to differences in the two instruments' observing strategies and sampling density. Figure 2B also illustrates the corresponding uncertainty in our analyses. The uncertainty is calculated using an ensemble technique (*71*) and further brings out the two phases in the time series of the Niño 3.4 X_{CO_2} anomaly: uncertainties of ±0.3 parts per million (ppm) during the El Niño onset phase with both the upper and lower bounds below the zero line, and larger uncertainties of ±0.5 ppm during the mature phase of the El Niño event. These larger uncertainties during the latter stages of the El Niño event illustrate the challenge in attributing the changes in X_{CO_2} anomalies to the competing, and often opposing, signals from the ocean and terrestrial components of the carbon cycle.

Attributing the two observed phases of X_{CO_2} anomalies to the ocean and the terrestrial response

Our argument for the two observed phases in the X_{CO_2} anomaly time series is supported by complementary data sources. The ocean response is corroborated by sea surface pCO_2 observations from an in situ network of autonomous CO_2 systems on the TAO moored buoy array (*9*, *38*, *75*). These data are not directly comparable to atmospheric X_{CO_2} as they describe CO_2 variations at the ocean surface. The trend of the difference between the sea surface and atmospheric CO_2 (ΔpCO_2), however, does capture typical El Niño signatures. For example, Fig. 2C illustrates data from one of the moored buoys in the Niño 3.4 region (0°, 170°W), which shows decreasing ΔpCO_2 over the spring months and near-zero ΔpCO_2 by December 2015. A suppression in the upwelling of CO_2-rich waters caused by weakening of the easterly trade winds leads to a reduction in the surface ocean carbon content, which in turn leads

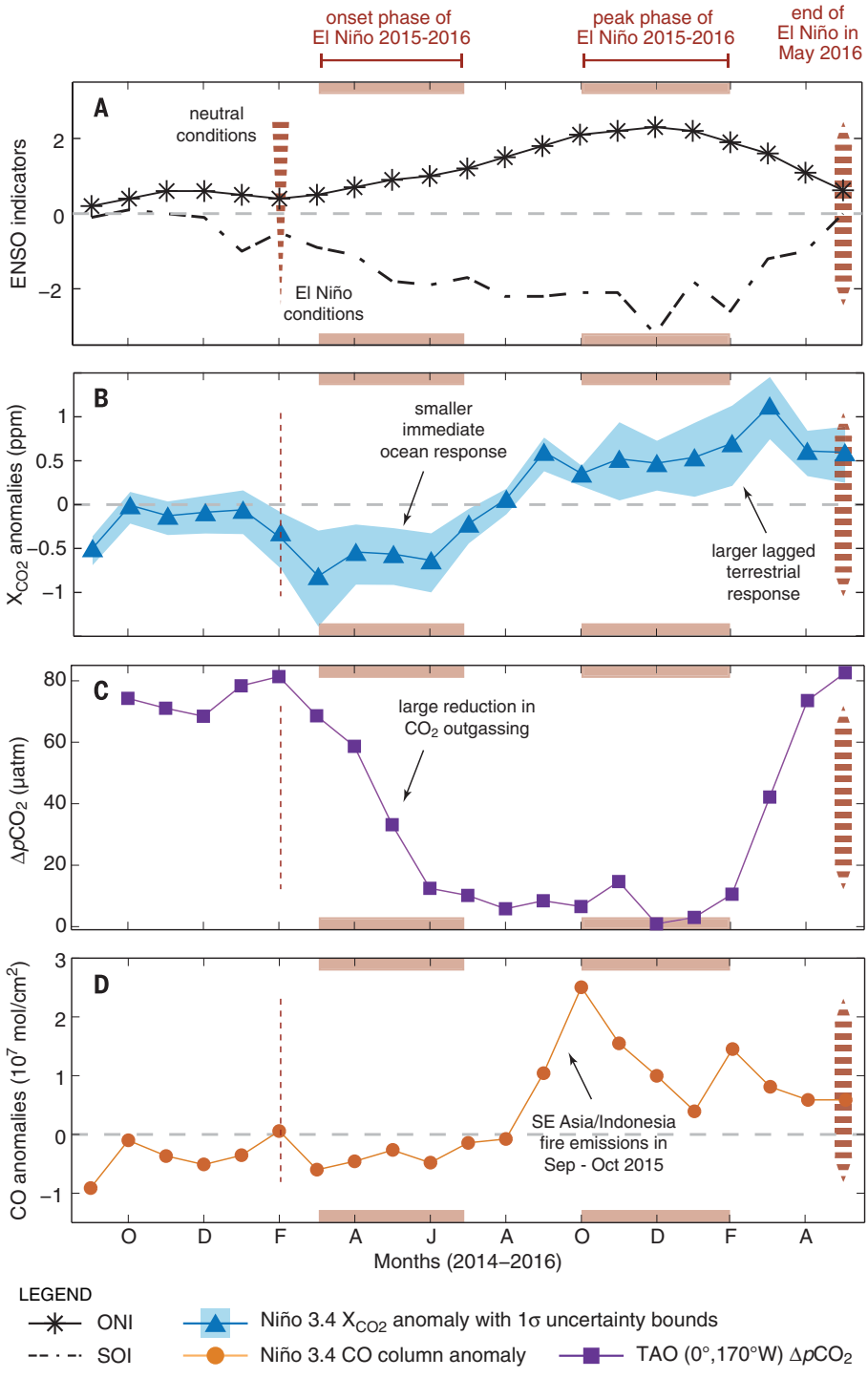

Fig. 2. OCO-2 observes the response of the carbon cycle for an entire El Niño event. (**A** to **D**) Temporal evolution of (A) the 2015–2016 El Niño as captured by the ONI and SOI indices; (B) X_{CO_2} anomalies and associated uncertainties in the Niño 3.4 region; (C) ΔpCO_2 from the TAO 0°, 170°W mooring; and (D) the CO total column anomalies in the Niño 3.4 region.

to a decline in the magnitude of sea-to-air CO_2 fluxes. The flux estimates at this buoy location are 1.35 ± 0.21 (1σ) g C m^{-2} month^{-1} during the November 2014–February 2015 period (i.e., non–El Niño conditions) that gradually decrease to 0.087 ± 0.083 (1σ) g C m^{-2} month^{-1} between November 2015 and February 2016 (i.e., El Niño conditions). This indicates a near-total shutdown of sea-to-air flux during boreal winter 2015–2016 relative to the neutral 2014–2015 boreal winter. Previous studies focusing on the tropical Pacific Ocean have reported flux reductions of ~40 to 60% over the entire basin (*9*–*12*, *33*, *36*, *63*, *68*). Atmospheric transport model calculations with a prescribed set of flux patterns (*71*) suggest a flux reduction of ~26 to 54%.

Although these numbers are roughly similar, we do recognize the limitation in comparing flux estimates from one point (namely the TAO location at 0°, 170°W) to flux estimates for the entire Niño 3.4 region and/or the tropical Pacific Ocean from previous studies. Large-scale changes in the physical and biogeochemical dynamics during El Niño events result in significant spatial and temporal variability in the surface pCO_2 distributions (*12*, *45*, *64*). Additionally, these spatial variations and their seasonal progression are uniquely tied to each El Niño event; thus, different types of El Niño events and/or shifts in the El Niño phenomena (*76*–*78*) will influence the evolution of the seasonal cycle of pCO_2 and air-sea CO_2 fluxes over the region. For the 2015–2016 El Niño event, the TAO buoy at 0°, 170°W lay closest to the edge of the warm pool and registered the first response to the onset of El Niño conditions. As observations from other TAO locations (*79*) are becoming available, it is evident that in the eastern part of the basin, there was an overall suppression of the outgassing CO_2 source but with large variability in pCO_2. Data synthesis and modeling work with these and other in situ observations are ongoing to quantify the exact magnitude of ocean CO_2 fluxes over different tropical Pacific regions during the 2015–2016 El Niño.

The second phase in the X_{CO_2} anomaly time series is driven by the terrestrial component of the carbon cycle and the transport of this signal to the remote Niño 3.4 region. The anomalous increase in CO_2 can be attributed to a combination of terrestrial sources, including a reduction in the global biospheric uptake, increases in soil and plant respiration, and enhanced fire emissions. Indeed, the impact of enhanced fire emissions and their regional progression was a well-studied feature following the strong 1997–1998 El Niño (*25*, *48*, *80*–*82*). For the 2015–2016 El Niño event, strong correspondences between X_{CO_2} from OCO-2 and the carbon monoxide (CO) total column anomalies from the Measurements of Pollution in the Troposphere (MOPITT) instrument on the NASA Terra platform are evident over the tropical Pacific Ocean, especially during fall 2015 (Fig. 2D). We conjecture that these CO total column anomalies are representative of the emissions from the 2015–2016 Indonesian peat fires (*83*–*86*), which were advected into the tropical Pacific region. El Niño–related changes in the Walker circulation (i.e., westerly winds) and the slightly more southern than normal positioning of the Intertropical Convergence Zone (*87*) may have allowed emissions from the Indonesian peat fires to carry over into this region (fig. S4).

Note that the positive increase in X_{CO_2} anomaly actually leads the fire signals by 1 to 2 months (Fig. 2, B and D). This indicates that the release of carbon flux resulting in an increase in CO_2 concentrations is only partially pyrogenic; reduced vegetation uptake due to droughts is an

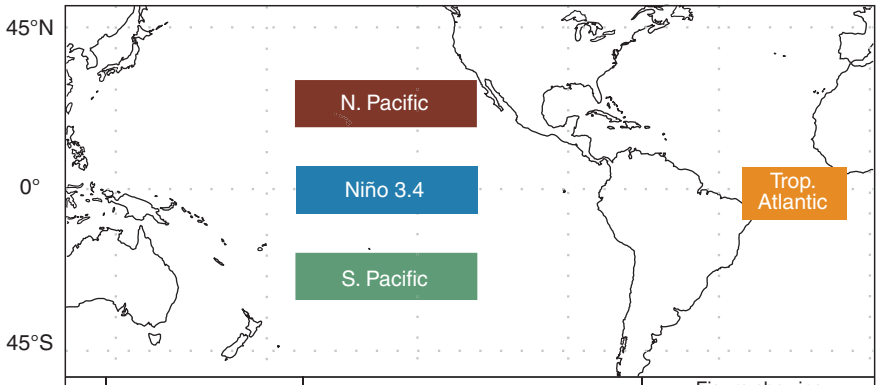

	Specific region analyzed	Alternative hypothesis	Figure showing difference between analyzed region and Niño 3.4
	Global (90°N -90°S, 0°-360°E)	X_{CO2} anomalies over the Pacific Ocean are responding to changes in terrestrial CO_2 concentrations	Fig. 4A
	Tropical Atlantic (5°N -5°S, 5°-35°W)	X_{CO2} anomalies over the Pacific Ocean are responding to changes in global CO_2 concentrations	Fig. 4B
	North Pacific (20°-30°N, 120°-170°W)	X_{CO2} anomalies over the tropical Pacific Ocean are responding to changes in CO_2 concentrations across the entire Pacific Ocean	Fig. 4C
	South Pacific (20°-30°S, 120°-170°W)	X_{CO2} anomalies over the tropical Pacific Ocean are responding to changes in CO_2 concentrations across the entire Pacific Ocean	Fig. 4C

Fig. 3. The specific ocean basins analyzed in this study. X_{CO_2} anomalies were calculated for the tropical Atlantic, North Pacific, and South Pacific basins and then compared with the X_{CO_2} anomalies from the Niño 3.4 region. Each of these regions was considered to accept or reject a specific hypothesis that could potentially bias the observed trend in the Niño 3.4 X_{CO_2} anomalies. After rejecting these hypotheses, we conclude that the negative X_{CO_2} anomaly observed over the Niño 3.4 region during the onset phase of El Niño 2015–2016 is unique and must be driven by local changes in the ocean fluxes.

important contributor, and quite possibly it is the initial cause of the increase in X_{CO_2} anomaly.

Isolating the observed negative X_{CO_2} anomaly to an ocean signal

The time dependence of the X_{CO_2} anomalies during the 2015–2016 El Niño indicates that the initial decrease in atmospheric CO_2 is due to suppression of upwelling in the tropical Pacific. This early negative response is subsequently offset by a large positive anomaly due to the terrestrial component. Assuming no significant interannual changes elsewhere in the global ocean, we can further confirm our argument by a comparison of the X_{CO_2} anomaly in the Niño 3.4 region with the global X_{CO_2} anomaly (Fig. 3 and Fig. 4A). By differencing the far-field effect from the local signal, the influence of the reduction in CO_2 outgassing from the tropical Pacific Ocean is clearly visible during the onset phase of El Niño. The peak reduction registered over the Niño 3.4 region relative to the global X_{CO_2} anomalies is 0.35 ppm in June 2015, which occurs a few months after the initiation of the El Niño event. Lag correlation of the Niño 3.4 X_{CO_2} anomalies against the ONI index indicates that the highest positive correlation occurs when the concentration-related anomalies lag the SST-related anomalies by 1 to 2 months (*88*) (fig. S8). The time lag relationship can be precisely quantified during the onset phase of El Niño, but it is much more difficult to interpret during the succeeding El Niño stages when any reduction in CO_2 from decreased equatorial upwelling is masked by the signal from terrestrial processes. Thus, if it were not for the reduction in outgassing from the ocean, the impact from the terrestrial sources would likely be larger. Our analysis confirms the findings from (*13*) that the slowdown of atmospheric CO_2 increase during the early stages of an El Niño event is indeed related to the decreased sea-to-air flux of CO_2 in the tropical Pacific Ocean. The coverage from the OCO-2 mission has enabled us to verify this hypothesis and monitor its temporal evolution using real atmospheric CO_2 observations.

The early-stage negative X_{CO_2} anomaly is unique to the tropical Pacific Ocean and is not influenced by global, terrestrial, or large–spatial scale fluxes. As a result of the large interhemispheric gradients in CO_2, typical variability in tropical CO_2 concentrations can be caused by terrestrial processes occurring at higher latitudes. To confirm that the recovered ocean signal in the X_{CO_2} anomaly is unique to the tropical Pacific Ocean, we examined three other ocean regions: the subtropical North Pacific (20° to 30°N, 120° to 170°W), the subtropical South Pacific (20° to 30°S, 120° to 170°W), and the tropical Atlantic Ocean (5°N to 5°S, 5° to 35°W). Figure 3 shows the specific regions (aside from Niño 3.4) that we have analyzed, each of which assists us in rejecting alternative hypotheses. Nonzero differences in X_{CO_2} anomalies between these and the Niño 3.4 region (Fig. 4) indicate that the trend observed over the tropical Pacific Ocean is distinct from other ocean basins. This makes intuitive sense from our mechanistic understanding as well: Although large impacts of the ENSO on the sea-to-air CO_2 flux in the tropical Pacific Ocean are expected, studies have shown minute and delayed influence of the ENSO modes on the variability of carbon fields in the tropical Atlantic Ocean (*67*, *89*, *90*).

Perspective

The strong El Niño in 2015–2016 caused a reduction in the magnitude of CO_2 outgassing from the tropical Pacific Ocean. These changes, albeit of varying magnitude, extended over a large portion of the tropical Pacific Ocean and affected the large-scale modulation of the physical processes responsible for the CO_2 efflux from this region. Almost all observing networks (i.e., OCO-2, TAO, etc.) were aided by the strength of this signal. However, OCO-2 provided a more comprehensive view of the tropical Pacific Ocean signal than previous observing networks because of (i) its greater coverage and more frequent sampling than in situ networks, and (ii) its improved resolution and precision relative to earlier space-based instruments. For example, GOSAT, like OCO-2, is sensitive to the total CO_2 column but has lower precision (single sounding random error of 2 ppm for GOSAT versus 0.5 ppm for OCO-2) and lower sampling density (fewer soundings by a factor of 100). The immediate next step will be to fold in these observations into an inverse modeling framework (*13*, *15*, *55*, *59*) to infer the underlying net fluxes between the ocean and atmosphere and between the terrestrial biosphere and atmosphere. This would help to establish the real benefit of OCO-2, especially against the backdrop of previous studies that had to rely on sparse atmospheric constraint to infer changes in CO_2 surface fluxes during El Niño events.

On the basis of OCO-2 data alone, however, we cannot quantitatively discriminate the relative roles of reduction in biospheric activity uptake due to a warmer and drier climate in 2015 versus enhanced fire emissions. Although we can quantify the temporal response of the ocean versus the terrestrial component and qualitatively observe the gradients in the response of different tropical Pacific Ocean regions (Fig. 5), it is much more challenging to discriminate the contribution of fire emissions and the delayed response of the terrestrial biosphere to El Niño–induced changes in weather patterns. The impact of ENSO is typically felt by the terrestrial biosphere over a period of several months to a year after the actual

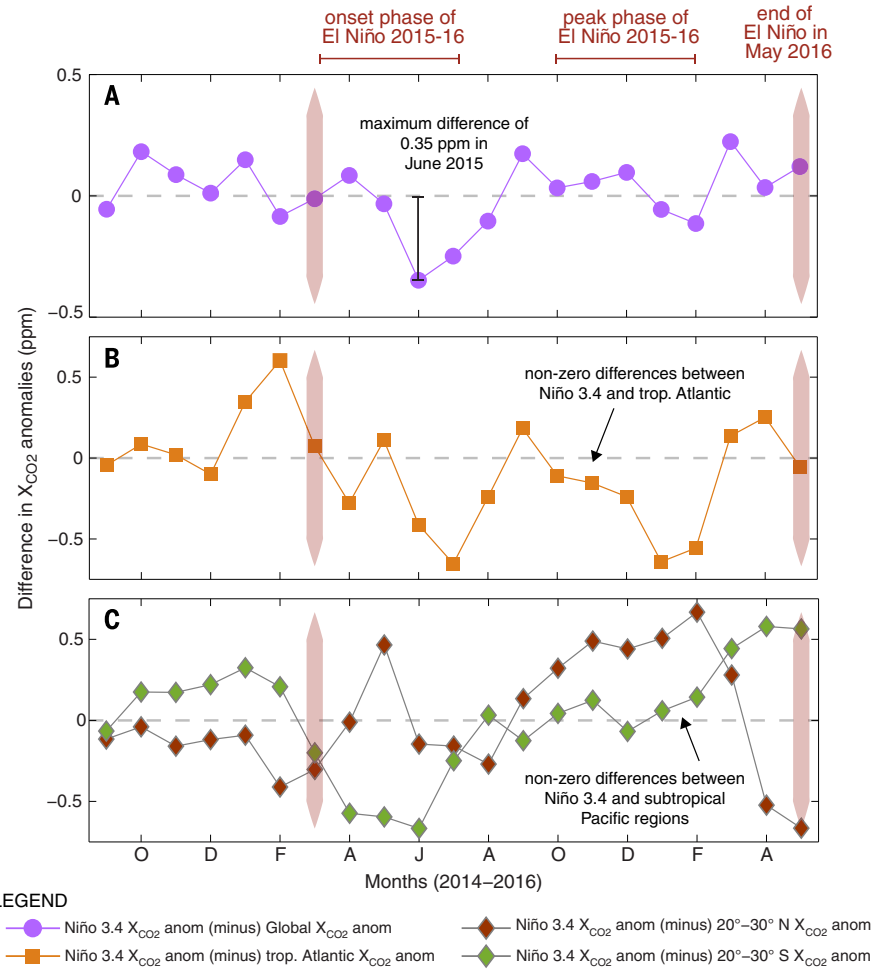

Fig. 4. Difference in X_{CO_2} anomalies between the Niño 3.4 region and other regions from September 2014 to May 2016. (**A**) The entire globe; (**B**) the tropical Atlantic Ocean; (**C**) the subtropical Pacific Ocean. See Fig. 3 for definitions of the regions. In (A), we see a robust pattern of negative X_{CO_2} anomaly between Niño 3.4 and the globe that is largest in 2015 and well synchronized with the onset phase of El Niño. In (B) and (C), nonzero differences between Niño 3.4 and the other ocean basins indicate that the Niño 3.4 trend is not reproducible in other ocean basins; this allows us to attribute the negative anomaly in Fig. 2B to a reduction in local CO_2 outgassing over the tropical Pacific Ocean.

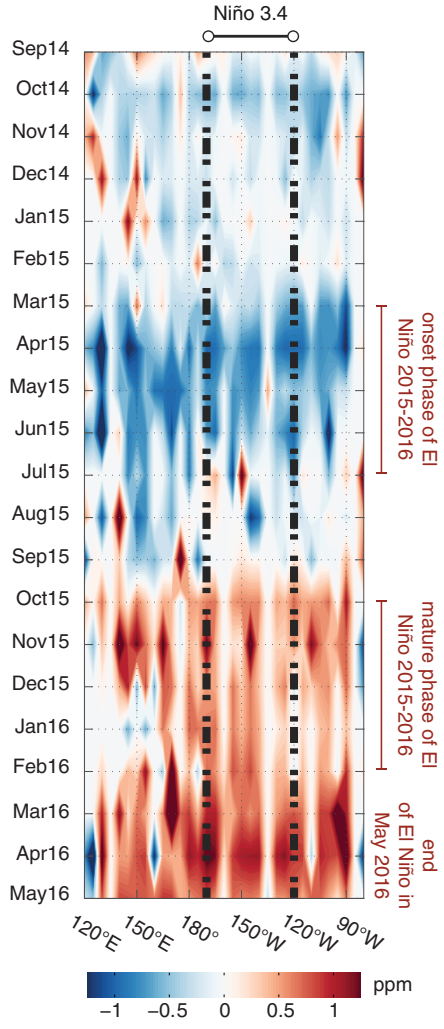

Fig. 5. Time evolution of the X_{CO_2} anomalies (ppm) averaged over 5°S to 5°N. The *x* axis represents longitude; the *y* axis shows the time progression in months. The 2015–2016 El Niño event and its onset and mature phases are highlighted to show the distinct responses observed over the tropical Pacific Ocean. The gray dot-dashed lines capture the boundaries of the Niño 3.4 region. During the onset phase (March to July 2015), perceptible gradients are observable from the far western Pacific to the central Pacific (consistent with the increasing flux from west to east) along with high variability in the X_{CO_2} anomalies in the central Pacific. Note that the X_{CO_2} anomalies are smaller over the eastern Pacific, which is consistent with surface seawater pCO_2 data collected on the TAO buoys (*79*). The transition from the ocean signal to the terrestrial signal happens between July and October 2015. Toward the latter stages of the El Niño event (i.e., November 2015 and later), the terrestrial signal dominates the observed trends in X_{CO_2}, likely masking any underlying ocean signal.

event. Studies on progressions of droughts (*91*) and fires (*25*) during an El Niño cycle have shown a hysteresis in the Earth system's response to changes in temperature and precipitation patterns. Analyses using ancillary data sources such as solar-induced fluorescence, bottom-up model simulations, and inverse modeling calculations are typically necessary to quantify the partitioning of the terrestrial carbon fluxes (reduction in biospheric uptake versus increase in fire emissions), as has been pursued in a companion study (*92*).

Our study provides a short-term perspective on the potential of CO_2 observations from space for unraveling more complex relationships of carbon sources and sinks. A longer time series of observations will enable the testing of more hypotheses, such as the possibility of regionally dependent gradients in air-sea CO_2 fluxes in the tropical Pacific, and will also support biogeochemical theories at previously inaccessible scales. From a long-term perspective, such information will improve our process-based understanding, inform our current suite of mechanistic models, and ultimately provide better constraints on future carbon cycle projections.

Concluding remarks

The strong El Niño event of 2015–2016 provided us with an opportunity to study how the global carbon cycle responds to changes in the physical climate system. With the high-resolution spatial and temporal observations available from OCO-2, we can directly observe the strong correlations that exist between atmospheric CO_2 concentrations and the El Niño signal. Moreover, the observations allow us to track the development of the atmospheric CO_2 anomaly as it switches from a negative phase (i.e., due to a reduction in CO_2 outgassing from the tropical Pacific Ocean) to a

strong positive phase (i.e., due to a reduction in biospheric uptake and increased fire emissions). The most important contribution of the space-based OCO-2 mission is the ability to observe and monitor carbon cycle phenomena at high density over large spatial scales, which has not been possible from the existing in situ network.

The complexity of the El Niño CO_2 signature illustrates that it is a multifaceted system with contributions from many regions and processes. Understanding and predicting its behavior requires separating out the many terrestrial and marine regions that contribute (*1*, *33*) and identifying both the geophysical (*3*, *27*, *30*) and the biological (*10*, *62*, *93*) phenomena that respond in their own unique ways. However, the impact on the carbon cycle is unified through the global mixing of CO_2 in the atmosphere. OCO-2 makes a valuable contribution by providing both the global coverage and fine surface spatial detail; the in situ CO_2 network of moorings and shipboard measurements provides the long-term climate quality record of atmospheric and ocean CO_2 observations and serves to validate the OCO-2 observations and model products. We emphasize that this diverse observing portfolio is necessary, and the complementary information provided by these observing systems will likely prove critical in understanding the partitioning of carbon fluxes during the 2015–2016 El Niño, the relative contribution of ocean versus land to the global atmospheric CO_2 growth rate, and the sensitivity of the carbon cycle to climate forcing on interannual to decadal time scales.

Materials and methods

X_{CO_2} retrievals from OCO-2 and GOSAT-ACOS

OCO-2 is NASA's first dedicated satellite mission for measuring column-average atmospheric X_{CO_2} with the accuracy, resolution, and coverage needed for quantifying CO_2 fluxes (sources and sinks) on regional scales over the globe (*70*, *94*, *95*). The X_{CO_2} retrievals used in this work are based on the version 7B level 2 algorithm. These data are freely available via the Goddard Earth Sciences Data and Information Services Center (GES DISC) from the start of mission operation. OCO-2 retrievals are also being cross-calibrated and cross-validated with measurements and data products from GOSAT (nicknamed "Ibuki"). The GOSAT X_{CO_2} retrievals used in this study were generated by version 7.3 of the ACOS algorithm [GOSAT-ACOS (*96*, *97*)]. Both OCO-2 and GOSAT-ACOS X_{CO_2} data were bias-corrected using the same set of predictors, so that these two satellite data sets could be combined to produce a uniform X_{CO_2} climate data record for use by the carbon cycle science community. See (*71*) for further details about the X_{CO_2} retrievals and the two satellite missions.

Generation of X_{CO_2} anomalies

Time series of X_{CO_2} (and, in general, any time series of atmospheric CO_2 concentrations) exhibit both a linear trend and a cyclostationary component due to the seasonal cycle. To account for the seasonality and the upward trend of CO_2, we adopted a two-step approach for generating the X_{CO_2} anomalies: (i) For each month, individual X_{CO_2} soundings from GOSAT-ACOS and OCO-2 are averaged over prespecified domains (e.g., Niño 3.4, tropical Pacific Ocean, tropical Atlantic Ocean, global) assuming no temporal correlation; and (ii) for an individual month, we find a linear trend that best fits the X_{CO_2} data from 7 years of GOSAT-ACOS and OCO-2 observational records for that month. The X_{CO_2} anomalies are then the residuals from this linear trend. See (*71*) for the exact mathematical framework and the implication for using both GOSAT-ACOS and OCO-2 together to generate the climatology.

pCO_2 observations from the TAO array

The TAO (Tropical Atmosphere Ocean) array of moored buoys in the tropical Pacific Ocean provides real-time, in situ meteorological and oceanographic measurements (*75*). Atmospheric and surface seawater partial pressure of CO_2 (pCO_2) is currently measured by moored autonomous pCO_2 ($MAPCO_2$) systems maintained on the TAO array at 0°, 110°W; 0°, 125°W; 0°, 140°W; 0°, 155°W; 0°, 170°W; 0°, 165°E; and 8°S, 165°E (*38*). The $MAPCO_2$ system also measures sample temperature, pressure, and relative humidity to calculate xCO_2 (dry) based on the equations in (*98*). SST and salinity data from TAO temperature and conductivity sensors are then used to calculate pCO_2 consistent with ocean carbon standard operating procedures as described in (*39*). Data plots from all TAO pCO_2 locations, which include both real time and finalized data, are available at www.pmel.noaa.gov/co2/story/Open+Ocean+Moorings. See (*71*) for details of the TAO array and the data set used in this study.

CO observations from the MOPITT instrument

Since March 2000, the MOPITT instrument on board the NASA/EOS Terra platform has been monitoring the CO content in the troposphere. Based on the recommendation of the MOPITT team, we use the Level 3 MOPITTv6 CO (*99*) estimated from the thermal-infrared (TIR) channel. For this study, we looked at the CO volume mixing ratio (VMR) for both the total column and at an individual atmospheric pressure level at 700 hPa during the period June 2002–May 2016. These data are freely available from the NASA Langley Research Center Atmospheric Science Data Center (https://eosweb.larc.nasa.gov/project/mopitt/mopitt_table). The climatological value of CO content in the atmosphere, and associated anomaly calculations for the study period, is based on this long and homogeneous CO data record (>14 years). See (*71*) for further details of the MOPITT instrument and its retrievals.

REFERENCES AND NOTES

1. M. J. McPhaden, S. E. Zebiak, M. H. Glantz, ENSO as an integrating concept in earth science. *Science* **314**, 1740–1745 (2006). doi: 10.1126/science.1132588; pmid: 17170296
2. S. G. Philander, *El Niño, La Niña, and the Southern Oscillation* (Academic Press, 1990).
3. J. D. Neelin *et al*., ENSO theory. *J. Geophys. Res.* **103**, 14261–14290 (1998). doi: 10.1029/97JC03424
4. K. E. Trenberth, The definition of El Niño. *Bull. Am. Meteorol. Soc.* **78**, 2771–2777 (1997). doi: 10.1175/1520-0477(1997)078<2771:TDOENO>2.0.CO;2
5. M. A. Cane, The evolution of El Niño, past and future. *Earth Planet. Sci. Lett.* **230**, 227–240 (2005). doi: 10.1016/j.epsl.2004.12.003
6. R. B. Bacastow *et al*., Atmospheric carbon dioxide, the southern oscillation, and the weak 1975 El Niño. *Science* **210**, 66–68 (1980). doi: 10.1126/science.210.4465.66; pmid: 17751153
7. C. D. Keeling, R. Revelle, Effects of El-Niño Southern Oscillation on the atmospheric content of carbon dioxide. *Meteoritics* **20**, 437–450 (1985).
8. C. D. Keeling, T. P. Whorf, M. Wahlen, J. van der Plichtt, Interannual extremes in the rate of rise of atmospheric carbon dioxide since 1980. *Nature* **375**, 666–670 (1995). doi: 10.1038/375666a0
9. F. P. Chavez *et al*., Biological and chemical response of the equatorial pacific ocean to the 1997-98 El Nino. *Science* **286**, 2126–2131 (1999). doi: 10.1126/science.286.5447.2126; pmid: 10591638
10. R. A. Feely, R. Wanninkhof, T. Takahashi, P. Tans, Influence of El Niño on the equatorial Pacific contribution to atmospheric CO_2 accumulation. *Nature* **398**, 597–601 (1999). doi: 10.1038/19273
11. R. A. Feely *et al*., Seasonal and interannual variability of CO_2 in the equatorial Pacific. *Deep Sea Res. II* **49**, 2443–2469 (2002). doi: 10.1016/S0967-0645(02)00044-9
12. R. A. Feely *et al*., Decadal variability of the air-sea CO_2 fluxes in the equatorial Pacific Ocean. *J. Geophys. Res.* **111**, C08S90 (2006). doi: 10.1029/2005JC003129
13. P. J. Rayner, R. M. Law, R. Dargaville, The relationship between tropical CO_2 fluxes and the El Niño-Southern Oscillation. *Geophys. Res. Lett.* **26**, 493–496 (1999). doi: 10.1029/1999GL900008
14. C. D. Jones, M. Collins, P. M. Cox, S. A. Spall, The carbon cycle response to ENSO: A coupled climate-carbon cycle model study. *J. Clim.* **14**, 4113–4129 (2001). doi: 10.1175/1520-0442(2001)014<4113:TCCRTE>2.0.CO;2
15. P. Peylin *et al*., Multiple constraints on regional CO_2 flux variations over land and oceans. *Global Biogeochem. Cycles* **19**, GB1011 (2005). doi: 10.1029/2003GB002214
16. K. R. Gurney, D. Baker, P. Rayner, S. Denning, Interannual variations in continental-scale net carbon exchange and sensitivity to observing networks estimated from atmospheric CO_2 inversions for the period 1980 to 2005. *Global Biogeochem. Cycles* **22**, GB3025 (2008). doi: 10.1029/2007GB003082
17. C. D. Nevison *et al*., Contribution of ocean, fossil fuel, land biosphere, and biomass burning carbon fluxes to seasonal and interannual variability in atmospheric CO_2. *J. Geophys. Res.* **113**, G01010 (2008). doi: 10.1029/2007JG000408
18. X. Jiang, M. T. Chahine, E. T. Olsen, L. L. Chen, Y. L. Yung, Interannual variability of mid-tropospheric CO_2 from Atmospheric Infrared Sounder. *Geophys. Res. Lett.* **37**, L13801 (2010). doi: 10.1029/2010GL042823
19. R. Betts, C. D. Jones, J. R. Knight, R. F. Keeling, J. J. Kennedy, El Niño and a record CO_2 rise. *Nat. Clim. Chang.* **6**, 806–810 (2016). doi: 10.1038/nclimate3063
20. P. M. Cox *et al*., Sensitivity of tropical carbon to climate change constrained by carbon dioxide variability. *Nature* **494**, 341–344 (2013). doi: 10.1038/nature11882; pmid: 23389447
21. K. E. Trenberth *et al*., Progress during TOGA in understanding and modeling global teleconnections associated with tropical sea surface temperatures. *J. Geophys. Res.* **103**, 14291–14324 (1998). doi: 10.1029/97JC01444
22. J. J. Tribbia, The rudimentary theory of atmospheric teleconnections associated with ENSO. In *Teleconnections Linking Worldwide Climate Anomalies*, M. H. Glantz, R. W. Katz, N. Nicholls, Eds. (Cambridge Univ. Press, 1991), pp. 285–308.
23. L. Resplandy, R. Séférian, L. Bopp, Natural variability of CO_2 and O_2 fluxes: What can we learn from centuries-long climate models simulations? *J. Geophys. Res.* **120**, 384–404 (2015). doi: 10.1002/2014JC010463
24. F. I. Woodward, M. R. Lomas, T. Quaife, Global responses of terrestrial productivity to contemporary climatic oscillations. *Philos. Trans. R. Soc. B* **363**, 2779–2785 (2008). doi: 10.1098/rstb.2008.0017; pmid: 18487132
25. Y. Le Page *et al*., Global fire activity patterns (1996-2006) and climatic influence: An analysis using the World Fire Atlas. *Atmos. Chem. Phys.* **8**, 1911–1924 (2008). doi: 10.5194/acp-8-1911-2008

26. A. Eldering *et al*., The Orbiting Carbon Observatory-2: First 18 months of science data products. *Atmos. Meas. Tech.* **10**, 549–563 (2017). doi: 10.5194/amt-10-549-2017
27. M. J. McPhaden, Playing hide and seek with El Niño. *Nat. Clim. Chang.* **5**, 791–795 (2015). doi: 10.1038/nclimate2775
28. A. F. Z. Levine, M. J. McPhaden, How the July 2014 easterly wind burst gave the 2015-2016 El Niño a head start. *Geophys. Res. Lett.* **43**, 6503–6510 (2016). doi: 10.1002/2016GL069204
29. F. Gasparin, D. Roemmich, The strong freshwater anomaly during the onset of the 2015/2016 El Niño. *Geophys. Res. Lett.* **43**, 6452–6460 (2016). doi: 10.1002/2016GL069542
30. H. Paek, J.-Y. Yu, C. Qian, Why were the 2015/2016 and 1997/1998 extreme El Niños different? *Geophys. Res. Lett.* **44**, 1848–1856 (2017). doi: 10.1002/2016GL071515
31. R. B. Bacastow, Modulation of atmospheric carbon dioxide by southern oscillation. *Nature* **261**, 116–118 (1976). doi: 10.1038/261116a0
32. R. E. Newell, B. C. Weare, A relationship between atmospheric carbon dioxide and Pacific sea surface temperatures. *Geophys. Res. Lett.* **4**, 1–2 (1977). doi: 10.1029/GL004i001p00001
33. J. L. Sarmiento, N. Gruber, Carbon cycle, CO_2 and climate. In *Ocean Biogeochemical Dynamics* (Princeton Univ. Press, 2006), pp. 392–453.
34. A. C. Manning, R. F. Keeling, L. E. Katz, W. J. Paplawsky, E. M. McEvoy, Interpreting the seasonal cycles of atmospheric oxygen and carbon dioxide concentrations at American Samoa Observatory. *Geophys. Res. Lett.* **30**, 1333 (2003). doi: 10.1029/2001GL014312
35. R. A. Feely, R. Wanninkhof, W. McGillis, M.-E. Carr, C. E. Cosca, Effects of wind speed and gas exchange parameterizations on the air-sea CO_2 fluxes in the equatorial Pacific Ocean. *J. Geophys. Res.* **109**, C08S03 (2004). doi: 10.1029/2003JC001896
36. M. Ishii *et al*., Air-sea CO_2 flux in the Pacific Ocean for the period 1990-2009. *Biogeosciences* **11**, 709–734 (2014). doi: 10.5194/bg-11-709-2014
37. C. D. Jones, P. M. Cox, On the significance of atmospheric CO_2 growth rate anomalies in 2002-2003. *Geophys. Res. Lett.* **32**, L14816 (2005). doi: 10.1029/2005GL023027
38. A. J. Sutton *et al*., Natural variability and anthropogenic change in equatorial Pacific surface ocean pCO_2 and pH. *Global Biogeochem. Cycles* **28**, 131–145 (2014). doi: 10.1002/2013GB004679
39. A. J. Sutton *et al*., A high-frequency atmospheric and seawater pCO_2 data set from 14 open-ocean sites using a moored autonomous system. *Earth Syst. Sci. Data* **6**, 353–366 (2014). doi: 10.5194/essd-6-353-2014
40. R. A. Feely *et al*., Distribution of chemical tracers in the eastern equatorial pacific during and after the 1982-1983 El Niño southern oscillation event. *J. Geophys. Res.* **92**, 6545–6558 (1987). doi: 10.1029/JC092iC06p06545
41. R. A. Feely, R. Wanninkhof, C. Goyet, D. E. Archer, T. Takahashi, Variability of CO_2 distributions and sea-air fluxes in the central and eastern equatorial Pacific during the 1991-1994 El Niño. *Deep Sea Res. II* **44**, 1851–1867 (1997). doi: 10.1016/S0967-0645(97)00061-1
42. A. M. E. Winguth *et al*., El Niño Southern Oscillation related fluctuations of the marine carbon cycle. *Global Biogeochem. Cycles* **8**, 39–63 (1994). doi: 10.1029/93GB03134
43. C. Le Quéré, J. C. Orr, P. Monfray, O. Aumont, G. Madec, Interannual variability of the oceanic sink of CO_2 from 1979 through 1997. *Global Biogeochem. Cycles* **14**, 1247–1265 (2000). doi: 10.1029/1999GB900049
44. M. C. Long, K. Lindsay, S. Peacock, J. K. Moore, S. C. Doney, Twentieth-century oceanic carbon uptake and storage in CESM1(BGC). *J. Clim.* **26**, 6775–6800 (2013). doi: 10.1175/JCLI-D-12-00184.1
45. V. K. Valsala, M. K. Roxy, K. Ashok, R. Murtugudde, Spatiotemporal characteristics of seasonal to multidecadal variability of pCO_2 and air-sea CO_2 fluxes in the equatorial Pacific Ocean. *J. Geophys. Res.* **119**, 8987–9012 (2014). doi: 10.1002/2014JC010212
46. A. Obata, Y. Kitamura, Interannual variability of the sea-air exchange of CO_2 from 1961 to 1998 simulated with a global ocean circulation-biogeochemistry model. *J. Geophys. Res.* **108**, 3337 (2003). doi: 10.1029/2001JC001088
47. H. Hashimoto *et al*., El Niño-Southern Oscillation-induced variability in terrestrial carbon cycling. *J. Geophys. Res.* **109**, D23110 (2004). doi: 10.1029/2004JD004959
48. P. K. Patra, M. Ishizawa, S. Maksyutov, T. Nakazawa, G. Inoue, Role of biomass burning and climate anomalies for land-atmosphere carbon fluxes based on inverse modeling of atmospheric CO_2. *Global Biogeochem. Cycles* **19**, GB3005 (2005). doi: 10.1029/2004GB002258
49. G. R. van der Werf *et al*., Interannual variability in global biomass burning emissions from 1997 to 2004. *Atmos. Chem. Phys.* **6**, 3423–3441 (2006). doi: 10.5194/acp-6-3423-2006
50. H. Qian, R. Joseph, N. Zeng, Response of the terrestrial carbon cycle to the El Niño-Southern Oscillation. *Tellus B* **60**, 537–550 (2008). doi: 10.1111/j.1600-0889.2008.00360.x
51. W. H. Li, P. Zhang, J. Ye, L. Li, P. A. Baker, Impact of two different types of El Niño events on the Amazon climate and ecosystem productivity. *J. Plant Ecol.* **4**, 91–99 (2011). doi: 10.1093/jpe/rtq039
52. T. Iguchi, Correlations between interannual variations of simulated global and regional CO_2 fluxes from terrestrial ecosystems and El Niño Southern Oscillation. *Tellus B* **63**, 196–204 (2011). doi: 10.1111/j.1600-0889.2010.00514.x
53. W. Wang *et al*., Variations in atmospheric CO_2 growth rates coupled with tropical temperature. *Proc. Natl. Acad. Sci. U.S.A.* **110**, 13061–13066 (2013). doi: 10.1073/pnas.1219683110; pmid: 23884654
54. W. R. L. Anderegg *et al*., Tropical nighttime warming as a dominant driver of variability in the terrestrial carbon sink. *Proc. Natl. Acad. Sci. U.S.A.* **112**, 15591–15596 (2015). doi: 10.1073/pnas.1521479112; pmid: 26644555
55. P. Bousquet *et al*., Regional changes in carbon dioxide fluxes of land and oceans since 1980. *Science* **290**, 1342–1347 (2000). doi: 10.1126/science.290.5495.1342; pmid: 11082059
56. C. R. Schwalm *et al*., Does terrestrial drought explain global CO_2 flux anomalies induced by El Niño? *Biogeosciences* **8**, 2493–2506 (2011). doi: 10.5194/bg-8-2493-2011
57. R. A. Feely *et al*., CO_2 distributions in the equatorial Pacific during the 1991–1992 ENSO event. *Deep Sea Res. II* **42**, 365–386 (1995). doi: 10.1016/0967-0645(95)00027-N
58. M. J. Behrenfeld *et al*., Biospheric primary production during an ENSO transition. *Science* **291**, 2594–2597 (2001). doi: 10.1126/science.1055071; pmid: 11283369
59. G. A. McKinley *et al*., Pacific dominance to global air-sea CO_2 flux variability: A novel atmospheric inversion agrees with ocean models. *Geophys. Res. Lett.* **31**, L22308 (2004). doi: 10.1029/2004GL021069
60. T. Takahashi *et al*., Climatological mean and decadal change in surface ocean pCO_2, and net sea-air CO_2 flux over the global oceans. *Deep Sea Res. II* **56**, 554–577 (2009). doi: 10.1016/j.dsr2.2008.12.009
61. G. H. Park *et al*., Variability of global net sea-air CO_2 fluxes over the last three decades using empirical relationships. *Tellus B* **62**, 352–368 (2010). doi: 10.1111/j.1600-0889.2010.00498.x
62. M. M. Gierach, T. Lee, D. Turk, M. J. McPhaden, Biological response to the 1997-98 and 2009-10 El Niño events in the equatorial Pacific Ocean. *Geophys. Res. Lett.* **39**, L10602 (2012). doi: 10.1029/2012GL051103
63. R. Wanninkhof *et al*., Global ocean carbon uptake: Magnitude, variability and trends. *Biogeosciences* **10**, 1983–2000 (2013). doi: 10.5194/bg-10-1983-2013
64. P. Landschützer, N. Gruber, D. C. E. Bakker, U. Schuster, Recent variability of the global ocean carbon sink. *Global Biogeochem. Cycles* **28**, 927–949 (2014). doi: 10.1002/2014GB004853
65. P. Landschützer, N. Gruber, D. C. E. Bakker, Decadal variations and trends of the global ocean carbon sink. *Global Biogeochem. Cycles* **30**, 1396–1417 (2016). doi: 10.1002/2015GB005359
66. C. Rödenbeck *et al*., Interannual sea-air CO_2 flux variability from an observation-driven ocean mixed-layer scheme. *Biogeosciences* **11**, 4599–4613 (2014). doi: 10.5194/bg-11-4599-2014
67. X. J. Wang, R. Murtugudde, E. Hackert, J. Wang, J. Beauchamp, Seasonal to decadal variations of sea surface pCO_2 and sea-air CO_2 flux in the equatorial oceans over 1984-2013: A basin-scale comparison of the Pacific and Atlantic Oceans. *Global Biogeochem. Cycles* **29**, 597–609 (2015). doi: 10.1002/2014GB005031
68. T. Takahashi, S. C. Sutherland, R. A. Feely, C. E. Cosca, Decadal variation of the surface water PCO_2 in the western and central equatorial Pacific. *Science* **302**, 852–856 (2003). doi: 10.1126/science.1088570; pmid: 14593175
69. S. Wenzel, P. M. Cox, V. Eyring, P. Friedlingstein, Emergent constraints on climate-carbon cycle feedbacks in the CMIP5 Earth system models. *J. Geophys. Res.* **119**, 794–807 (2014). doi: 10.1002/2013JG002591
70. D. Crisp *et al*., The on-orbit performance of the Orbiting Carbon Observatory-2 (OCO-2) instrument and its radiometrically calibrated products. *Atmos. Meas. Tech.* **10**, 59–81 (2017). doi: 10.5194/amt-10-59-2017
71. See supplementary materials.
72. D. Wunch *et al*., Comparisons of the Orbiting Carbon Observatory-2 (OCO-2) X_{CO2} measurements with TCCON. *Atmos. Meas. Tech.* **10**, 2209–2238 (2017). doi: 10.5194/amt-10-2209-2017
73. See the full list at www.esrl.noaa.gov/psd/data/climateindices/list.
74. A. Kuze, H. Suto, M. Nakajima, T. Hamazaki, Thermal and near infrared sensor for carbon observation Fourier-transform spectrometer on the Greenhouse Gases Observing Satellite for greenhouse gases monitoring. *Appl. Opt.* **48**, 6716–6733 (2009). doi: 10.1364/AO.48.006716; pmid: 20011012
75. M. J. McPhaden *et al*., The tropical ocean global atmosphere observing system: A decade of progress. *J. Geophys. Res.* **103**, 14169–14240 (1998). doi: 10.1029/97JC02906
76. J.-S. Kug, F. F. Jin, S. An, Two types of El Niño events: Cold tongue El Niño and warm pool El Niño. *J. Clim.* **22**, 1499–1515 (2009). doi: 10.1175/2008JCLI2624.1
77. K. Ashok, T. Yamagata, Climate change: The El Niño with a difference. *Nature* **461**, 481–484 (2009). doi: 10.1038/461481a; pmid: 19779440
78. M. J. McPhaden, T. Lee, D. McClurg, El Niño and its relationship to changing background conditions in the tropical Pacific Ocean. *Geophys. Res. Lett.* **38**, L15709 (2011). doi: 10.1029/2011GL048275
79. Data from other TAO locations (for example, at 0°, 110°W) demonstrate the heterogeneity in CO_2 concentrations as we move from west-to-east over the tropical Pacific Ocean. These data can be viewed at www.pmel.noaa.gov/co2/story/OpenOceanMoorings.
80. S. E. Page *et al*., The amount of carbon released from peat and forest fires in Indonesia during 1997. *Nature* **420**, 61–65 (2002). doi: 10.1038/nature01131; pmid: 12422213
81. R. L. Langenfelds *et al*., Interannual growth rate variations of atmospheric CO_2 and its $\delta^{13}C$, H_2, CH_4, and CO between 1992 and 1999 linked to biomass burning. *Global Biogeochem. Cycles* **16**, 1048–1069 (2002). doi: 10.1029/2001GB001466
82. G. R. van der Werf *et al*., Continental-scale partitioning of fire emissions during the 1997 to 2001 El Niño/La Niña period. *Science* **303**, 73–76 (2004). doi: 10.1126/science.1090753; pmid: 14704424
83. R. J. Parker *et al*., Atmospheric CH_4 and CO_2 enhancements and biomass burning emission ratios derived from satellite observations of the 2015 Indonesian fire plumes. *Atmos. Chem. Phys.* **16**, 10111–10131 (2016). doi: 10.5194/acp-16-10111-2016
84. V. Huijnen *et al*., Fire carbon emissions over maritime southeast Asia in 2015 largest since 1997. *Sci. Rep.* **6**, 26886 (2016). doi: 10.1038/srep26886; pmid: 27241616
85. R. D. Field *et al*., Indonesian fire activity and smoke pollution in 2015 show persistent nonlinear sensitivity to El Niño-induced drought. *Proc. Natl. Acad. Sci. U.S.A.* **113**, 9204–9209 (2016). doi: 10.1073/pnas.1524888113; pmid: 27482096
86. Y. Yin *et al*., Variability of fire carbon emissions in equatorial Asia and its nonlinear sensitivity to El Niño. *Geophys. Res. Lett.* **43**, 10472–10479 (2016). doi: 10.1002/2016GL070971
87. T. Schneider, T. Bischoff, G. H. Haug, Migrations and dynamics of the intertropical convergence zone. *Nature* **513**, 45–53 (2014). doi: 10.1038/nature13636; pmid: 25186899
88. Bacastow (*31*) found the lag between one of the El Niño indices (SOI) and the CO_2 concentration changes to be 2.5 months at Mauna Loa and 6 months at South Pole. Rayner *et al*. (*13*) found in their study that CO_2 data anomalies lag the SOI by one month. Later, Jones *et al*. (*14*) claimed that Mauna Loa CO_2 lagged behind Niño 3 SST anomalies by 3 months. The handful of studies illustrate the range of ENSO indices and atmospheric CO_2 dataset that have been used; however, all of these studies were impacted by a lack of broad-scale observations over the tropical Pacific during the different phases of an El Niño event. This study provides a refinement of these earlier estimates of the time lags using higher-density space-based observations.
89. G. A. McKinley, A. R. Fay, T. Takahashi, N. Metzl, Convergence of atmospheric and North Atlantic carbon dioxide trends on multidecadal timescales. *Nat. Geosci.* **4**, 606–610 (2011). doi: 10.1038/ngeo1193
90. N. Lefèvre, G. Caniaux, S. Janicot, A. K. Gueye, Increased CO_2 outgassing in February-May 2010 in the tropical Atlantic following the 2009 Pacific El Niño. *J. Geophys. Res.* **118**, 1645–1657 (2013). doi: 10.1002/jgrc.20107
91. S. M. Vicente-Serrano *et al*., A multiscalar global evaluation of the impact of ENSO on droughts. *J. Geophys. Res.* **116**, D20109 (2011). doi: 10.1029/2011JD016039
92. J. Liu *et al*., Contrasting carbon cycle responses of the tropical continents to the 2015–2016 El Niño. *Science* **358**, eaam5690 (2017).

93. C. Pala, Corals tie stronger El Niños to climate change. *Science* **354**, 1210 (2016). doi: 10.1126/science.354.6317.1210; pmid: 27940821
94. D. Crisp *et al*., The Orbiting Carbon Observatory (OCO) mission. *Adv. Space Res.* **34**, 700–709 (2004). doi: 10.1016/j.asr.2003.08.062
95. R. Pollock *et al*., The Orbiting Carbon Observatory instrument: Performance of the OCO instrument and plans for the OCO-2 instrument. *Proc. SPIE* **7826**, 78260W (2010). doi: 10.1117/12.865243
96. C. O'Dell *et al*., The ACOS CO_2 retrieval algorithm—Part 1: Description and validation against synthetic observations. *Atmos. Meas. Tech.* **5**, 99–121 (2012). doi: 10.5194/amt-5-99-2012
97. D. Crisp *et al*., The ACOS CO_2 retrieval algorithm—Part II: Global X_{CO2} data characterization. *Atmos. Meas. Tech.* **5**, 687–707 (2012). doi: 10.5194/amt-5-687-2012
98. R. F. Weiss, Carbon dioxide in water and seawater: The solubility of a non-ideal gas. *Mar. Chem.* **2**, 203–215 (1974). doi: 10.1016/0304-4203(74)90015-2
99. M. N. Deeter *et al*., The MOPITT Version 6 product: Algorithm enhancements and validation. *Atmos. Meas. Tech.* **7**, 3623–3632 (2014). doi: 10.5194/amt-7-3623-2014

ACKNOWLEDGMENTS

This work was supported by funding from the NASA ROSES-2014 Grant/Cooperative Agreement NNX15AG92G. A portion of this research was carried out at the Jet Propulsion Laboratory (JPL), California Institute of Technology, under a contract with NASA. The work of B.B.S. was supported by the National Center for Atmospheric Research (NCAR), which is sponsored by NSF. The work of A.J.S. and R.A.F. was funded by the NOAA Office of Oceanic and Atmospheric Research, including resources from the Ocean Observation and Monitoring Division of the Climate Program Office (FundRef no. 100007298). This is Pacific Marine Environmental Laboratory Contribution no. 4607. The OCO-2 and GOSAT-ACOS data were produced by the ACOS/OCO-2 project at JPL and were obtained from the free ACOS/OCO-2 data archive maintained at GES DISC (https://disc.gsfc.nasa.gov/OCO-2). The MOPITT data sets were obtained from the NASA Langley Research Center Atmospheric Science Data Center (https://eosweb.larc.nasa.gov/project/mopitt/mopitt_table). We thank the National Data Buoy Center for supporting deployment and recovery of the moored pCO_2 systems and maintenance of the TAO buoys; three anonymous reviewers for their comments; and H. Worden (NCAR), J. Worden (JPL), P. Wennberg (Caltech), S. Pawson (NASA), S. Cohn (NASA), L. Ott (NASA), and B. Weir (USRA) for discussions; and D. Hinkle (JPL) and S. Spangler (Science Systems and Applications Inc.) for help with graphic design.

SUPPLEMENTARY MATERIALS

www.sciencemag.org/content/358/6360/eaam5776/suppl/DC1
Materials and Methods
Supplementary Text
Figs. S1 to S8
Table S1
References (*100*–*124*)

12 December 2016; accepted 7 July 2017
10.1126/science.aam5776

Influence of El Niño on atmospheric CO_2 over the tropical Pacific Ocean: Findings from NASA's OCO-2 mission

A. Chatterjee, M. M. Gierach, A. J. Sutton, R. A. Feely, D. Crisp, A. Eldering, M. R. Gunson, C. W. O'Dell, B. B. Stephens and D. S. Schimel

Science **358** (6360), eaam5776.
DOI: 10.1126/science.aam5776